Quantum many-body intermetallics: Phase stability of Fe_3Al and small-gap formation in Fe_2VAl

Oleg Kristanovski,[1] Raphael Richter,[2] Igor Krivenko,[1] Alexander I. Lichtenstein,[1] and Frank Lechermann[1,3]
[1]*I. Institut für Theoretische Physik, Universität Hamburg, D-20355 Hamburg, Germany*
[2]*Institut für Technische Thermodynamik, Deutsches Zentrum für Luft- und Raumfahrt, D-70569 Stuttgart*
[3]*Institut für Keramische Hochleistungswerkstoffe, Technische Universität Hamburg-Harburg, D-21073 Hamburg, Germany*
(Received 22 September 2016; published 10 January 2017)

Various intermetallic compounds harbor subtle electronic correlation effects. To elucidate this fact for the Fe-Al system, we perform a realistic many-body investigation based on a combination of density functional theory with dynamical mean-field theory in a charge self-consistent manner. A better characterization and understanding of the phase stability of bcc-based $D0_3$-Fe_3Al through an improved description of the correlated charge density and the magnetic energy is achieved. Upon replacement of one Fe sublattice with V, the Heusler compound Fe_2VAl is realized, known to display bad-metal behavior and increased specific heat. Here we document a charge-gap opening at low temperatures in line with previous experimental work. The gap structure does not match conventional band theory and is reminiscent of (pseudo)gap characteristics in correlated oxides.

DOI: 10.1103/PhysRevB.95.045114

I. INTRODUCTION

The Fe-Al system is well known for its intricate phase diagram, displaying a complex interplay between metallicity, magnetism, and structure. Stoichiometric FeAl poses a longstanding problem regarding its magnetic ground state. While experimentally $B2$-FeAl is characterized as a Curie-Weiss paramagnet [1] with no detectable ordered moment, conflicting results exist in theory [2–5]. On the Al-rich side, the low-symmetry structures $FeAl_2$ and Fe_2Al_5 exhibit spin-glass physics at low temperature [6,7]. On the iron-rich side, in the Fe_3Al composition a bcc-based $D0_3$ crystal structure is stable with well-defined ferromagnetic (FM) order up to $T_c = 713$ K [8]. A further increase of the Fe content transforms the system into a doped bcc Fe (or α) phase, also with FM order below a Curie temperature of 1043 K for pure iron. Albeit unambiguous in nature, both α-Fe and $D0_3$-Fe_3Al appear difficult to be described within conventional density functional theory (DFT) [9–11]. The generalized-gradient approximation (GGA) for the exchange-correlation energy is necessary to detect the FM-bcc-Fe ground state [10]. Intriguingly, the FM-$D0_3$ compound is only stable within the local-density approximation (LDA), while GGA favors the fcc-based $L1_2$ structure in the ferromagnetic state [11].

This lack of a coherent theoretical description of the Fe-rich side of Fe-Al in standard Kohn-Sham DFT asks for extended approaches. The inclusion of static electronic correlation effects via the DFT+Hubbard U method may cope with part of the subtle energetics for a reasonable choice of the local Coulomb-interaction parameters [12]. But that scheme is in principle not well defined for correlated itinerant systems and, in addition, usually needs to enforce magnetic order to deliver proper results. True paramagnetic (PM) states based on fluctuating local moments are neither accessible in conventional DFT nor in DFT+U, which either describes nonmagnetic (NM) or magnetically ordered compounds. Within the so-called disordered local moment (DLM) method [13,14] there is the chance to account for a DFT-based orientational mean-field effect of PM-like spins. Yet quantum fluctuations as well as general finite-temperature fluctuations of, e.g., the proper size of the local moments are still missing.

A further facet of the intriguing correlated electronic structure in iron aluminides is revealed when replacing one Fe sublattice in $D0_3$-Fe_3Al with vanadium. This transforms the intermetallic crystal into the Heusler $L2_1$ compound Fe_2VAl. The ordered alloy is paramagnetic down to lowest temperatures and displays bad-metal behavior in transport [15]. It is still a matter of debate if Fe_2VAl is a small-gap ($\sim$0.1–0.3 eV) semiconductor or a semimetal [16,17]. Reminiscent of f-electron systems such as SmB_6 with Kondo-insulating characteristics [18], heavy-fermion physics was originally associated with this $3d$-electron system [15,16]. Though magnetic defects later explained a sizable part of the large specific heat at low temperature, the overall mass enhancement remains substantial [19]. A promising thermoelectric potential due to an enhanced thermopower is associated with Fe_2VAl-based materials [20,21]. Again, a theoretical first-principles assessment is difficult, since, e.g., there are substantial differences concerning the existence of a charge gap Δ and its eventual size. Conventional DFT based on LDA/GGA classifies Fe_2VAl as semimetallic [22,23], whereas the use of hybrid functionals renders the system semiconducting with a band gap of $\Delta_g = 0.34$ eV [24]. A gap of $\Delta_g = 0.55$ eV is revealed from DFT+U calculations [25].

In this paper a first-principles many-body approach is employed to consider the effects of quantum fluctuations and finite temperature on the electronic structure of Fe_3Al and Fe_2VAl beyond conventional DFT(+U). A state-of-the-art combination of density functional theory with dynamical mean-field theory (DMFT) reveals important modifications of the correlated electronic structure. We show that the subtle electronic states rely on many-electron quantum processes, with important consequences for the phase stability and tendencies concerning gap formation. This paves the way towards a coherent modeling and understanding of Fe-Al and signals the general importance of advanced theoretical schemes for intermetallic systems.

II. CRYSTAL STRUCTURES

The crystal structures relevant for this work are displayed in Fig. 1. With bcc Fe and fcc Al as the end members, the

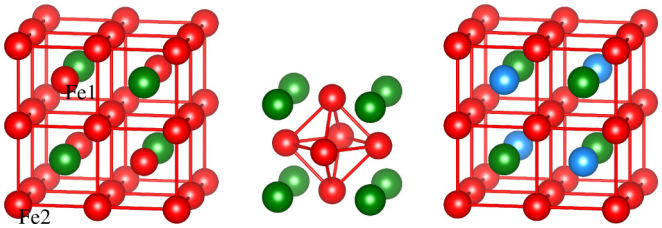

FIG. 1. Relevant crystal structures. From left to right: $D0_3$-Fe_3Al, $L1_2$-Fe_3Al, and $L2_1$-Fe_2VAl. Fe (red/light gray), Al (green/dark), and V (blue/gray).

cubic lattice system also accounts for the dominant ordered phases in Fe-Al. Starting with $B2$-FeAl at stoichiometry, the bcc lattice is the common host for the stable solid phases in the Fe-rich part. Though the $D0_3$ structure is stable in the Fe_3Al phase regime, the fcc-based $L1_2$ structure appears as a relevant competitor. The $D0_3$ unit cell consists of three Fe sites and one Al site, whereby the Fe basis atoms are grouped in two symmetry shells. One Fe site belongs to the Fe1 sublattice and two Fe sites to the Fe2 sublattice. As a bcc structure, each Fe site has eight nearest-neighbor (NN) sites. Whereas the Fe2 atoms have a mixed Fe/Al nearest neighborhood, the Fe1 atom has only Fe nearest neighbors. The experimental lattice constant of fully ordered Fe_3Al reads $a = 5.473$ a.u.

The $L1_2$ structure also consists of three Fe atoms and one Al atom in the primitive unit cell, but all Fe sites are equivalent by symmetry. The 12-atom NN shell of these Fe sites is composed again of both Fe and Al sites.

Finally, in the Heusler $L2_1$-Fe_2VAl compound, the Fe1 sublattice of the $D0_3$ structure is fully replaced with V atoms. The measured lattice constant amounts to $a' = 5.442$ a.u. [15,16].

Note that throughout this work we investigate the stoichiometric compounds, i.e., the defect physics and effects of chemical disorder are not treated.

III. COMPUTATIONAL FRAMEWORK

The charge self-consistent DFT+DMFT methodology [26–28] is put into practice, utilizing a mixed-basis pseudopotential approach [29,30] for the DFT part and the continuous-time quantum Monte Carlo scheme [31,32] from the TRIQS package [33,34] for the DMFT impurity treatment. Exchange correlation in the Kohn-Sham cycle is handled by the GGA functional of Perdew-Burke-Ernzerhof (PBE) [35] form.

The correlated subspace where quantum fluctuations are explicitly accounted for is associated with the transition-metal sites of Fe and V types. Projected local orbitals [36–40] of a $3d$ character are used to extract Wannier-like states based on 22 Kohn-Sham bands, stemming from Fe/V($3d\,4s$) and Al($3s\,3p$) orbitals. Each transition-metal site represents a DMFT impurity problem, which, due to symmetry, amounts to two such ones in $D0_3$-Fe_3Al and Fe_2VAl, while only one symmetry-inequivalent transition-metal site is hosted in $L1_2$-Fe_3Al. A multiorbital Hubbard Hamiltonian of Slater-Kanamori form, parametrized by the Hubbard U and the Hund's exchange J_H, is applied to the respective full five-orbital $3d$ manifold. We overtook the values $U = 3.36$ eV and $J_H = 0.71$ eV for the local Coulomb interactions from Ref. [5], where those are computed for $B2$-FeAl using the constrained random-phase approximation. A double-counting correction of the fully localized form is used in this work. If not stated otherwise, the temperature within the DMFT part is set to $T = 387$ K, i.e., $\beta = 1/T = 30\ \mathrm{eV}^{-1}$. The analytical continuation of the Green's functions on the Matsubara axis $i\omega$ is performed via the maximum-entropy method.

We mainly focus in our DMFT calculations on phases without broken spin symmetry, i.e., paramagnetic states. Albeit $D0_3$-Fe_3Al is ferromagnetic at ambient temperatures, the explicit magnetic-*ordering* energy, as will be shown below, is not of vital importance for our investigation and its conclusions.

IV. RESULTS

A. Fe_3Al

1. *Electronic states*

We first focus in some detail on the electronic states in Fe_3Al. Let us start with the fcc-based $L1_2$ structure, having only one transition-metal sublattice. The close-packed lattice type is an important one in intermetallic systems, e.g., the ordered phases Cu_3Au and Ni_3Al condense in the $L1_2$ structure. Because of the cubic symmetry, here the local Fe($3d$) states in principle split twofold into e_g and t_{2g} states. However, due to the ordering pattern, not all e_g/t_{2g} sublevels may still be degenerate. This is illustrated in Fig. 2, where the obtained Fe($3d$) projected local orbitals are plotted as isosurfaces. The e_g manifold consisting of $\{x^2 - y^2, z^2\}$ is defined by the orbital lobes pointing towards the next-nearest-neighboring (NNN) Fe sites. Since both pointing directions are anisotropic in terms of the respective nearest-neighbor sites, the two e_g are nondegenerate. The t_{2g} manifold consisting of $\{xz, yz, xy\}$ are defined by the orbital lobes pointing to the NN sites. For xz, yz the associated NN sites are exclusively of a Fe type, therefore both orbitals are degenerate. Yet in the case of xy, the associated NN shell consists exclusively of Al sites, thus this t_{2g} orbital has a different, in fact, the lowest effective, crystal-field level.

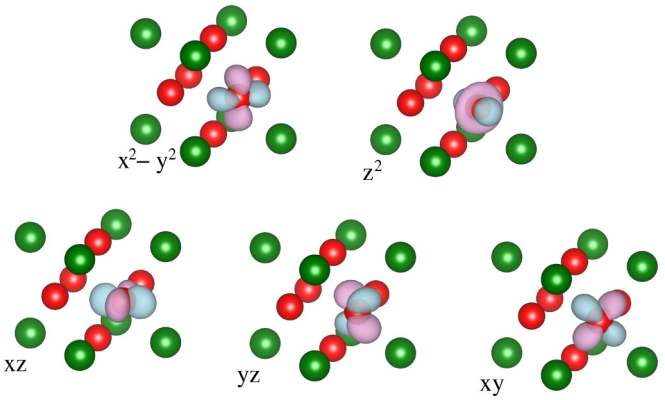

FIG. 2. Projected local Fe($3d$) orbitals in $L1_2$-Fe_3Al. On-site level energies: $\varepsilon_\alpha = \{-624, -699, -843, -843, -998\}$ meV for the effective orbitals $\alpha = \{x^2 - y^2, z^2, xz, yz, xy\}$.

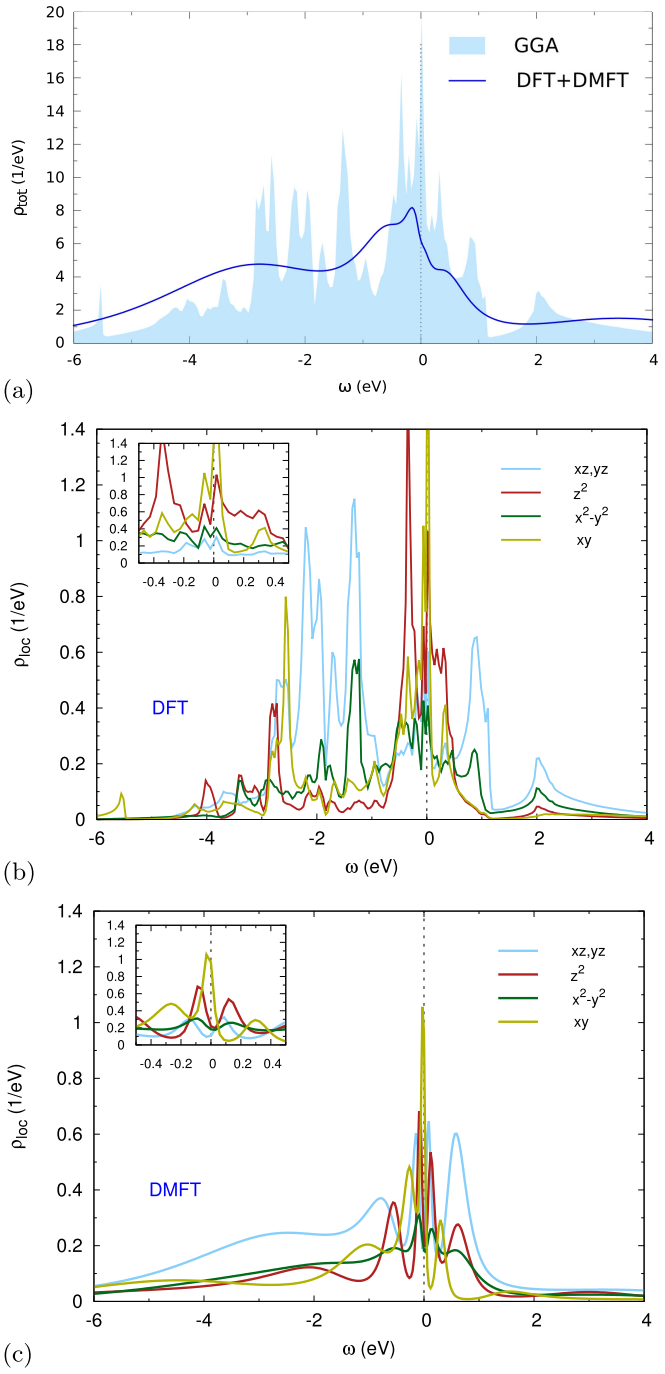

FIG. 3. Spectral functions of $L1_2$-Fe_3Al. (a) Total, (b) local Fe from GGA, and (c) local Fe from DFT+DMFT. Insets in (b) and (c) are low-energy blowups.

Figure 3 compares the integrated spectral functions $\rho(\omega) = \sum_{\mathbf{k}} A(\mathbf{k},\omega)$ of $L1_2$-Fe_3Al within DFT(GGA) and DFT+DMFT. From the broadly itinerant band structure, an effective relevant bandwidth of about 7 eV (ranging from -6 to 1 eV) may be read off. Seemingly, the full Fe($3d$) manifold is crucial to understand the electronic structure in the bonding part and at low energy, since the hybridization between Fe and Al is rather strong in a wide energy range. Close to the Fermi level, the z^2 and xy effective orbitals are most dominant in GGA, while, e.g., the xz/yz part displays a bonding-antibonding signature.

TABLE I. Projected local-orbital occupations in Fe_3Al. The first rows are GGA, and the second rows DFT+DMFT results, respectively.

		e_g		t_{2g}			
		x^2-y^2	z^2	xz	yz	xy	Total
$L1_2$	Fe	1.38	1.34	1.43	1.43	1.58	7.16
		1.55	1.56	1.54	1.54	1.79	7.98
$D0_3$	Fe1	1.45	1.45	1.31	1.31	1.31	6.83
		1.47	1.47	1.54	1.54	1.54	7.56
	Fe2	1.20	1.20	1.59	1.59	1.59	7.17
		1.45	1.45	1.70	1.70	1.70	8.00

For the xy state with a deepest crystal-field level and broad dispersion, the orbital filling is also largest (see Table I). The total local Fe electron count is slightly above seven within GGA. A further strengthening of the xy dominance at low energy occurs in the DFT+DMFT treatment. While the filling of all effective Fe orbitals increases with correlations, here also the occupation of the xy state is enhanced the most by relative means. Overall, a substantial increase in the total effective Fe($3d$) filling close to eight electrons takes place. Note that the site-filling differences between GGA and DFT+DMFT are also due to the respective effective-orbital definitions, as usual in determining local occupations in crystalline solids. First, the projected local orbitals in both calculational schemes are not identical (only the projecting functions are), since via the charge self-consistent loop the Kohn-Sham part (i.e., the bands used for the projection) changes. Second, the resulting orbitals are of a Wannier type, i.e., their spread is substantial and not localized on the site center within a small spherical radius.

Still, correlations may enhance the electron localization on the Fe sites. The correlation strength can be estimated from the quasiparticle (QP) weight $Z \sim 1/m_{\text{eff}}$, computed from the electronic self-energy on the Matusbara axis as

$$Z = \left(1 - \left.\frac{\partial\, \mathrm{Im}\, \Sigma(i\omega)}{\partial\omega}\right|_{\omega\to 0^+}\right)^{-1}. \qquad (1)$$

There is no strong orbital variation of the QP weight in the $L1_2$ structure and it amounts to a moderate value of $Z \sim 0.7$.

Though the $D0_3$ structure consists of two different Fe sublattices, the conventional internal degeneracies of the e_g and t_{2g} subshells of Fe($3d$) are fulfilled here. This is due to the fact that the NN environments are either of a pure Fe type or of an equally mixed-isotropic Fe,Al type. As in fcc-based $L1_2$, the e_g orbitals point again towards NN and NNN sites. However, since bcc-based $D0_3$ is not close packed, the t_{2g} orbitals point in between the NN and NNN, i.e., towards the third-nearest-neighbor sites.

The total integrated spectral function of $D0_3$-Fe_3Al is similar to the one of $L1_2$-Fe_3Al [see Fig. 4(a)], but with a more pronounced quasiparticle peak at low energy. The effective relevant bandwidth seems also smaller by about 1 eV in extent. On the local level, the Fe1 spectrum exhibits stronger e_g-t_{2g} discrimination than the Fe2 spectrum. This speaks to

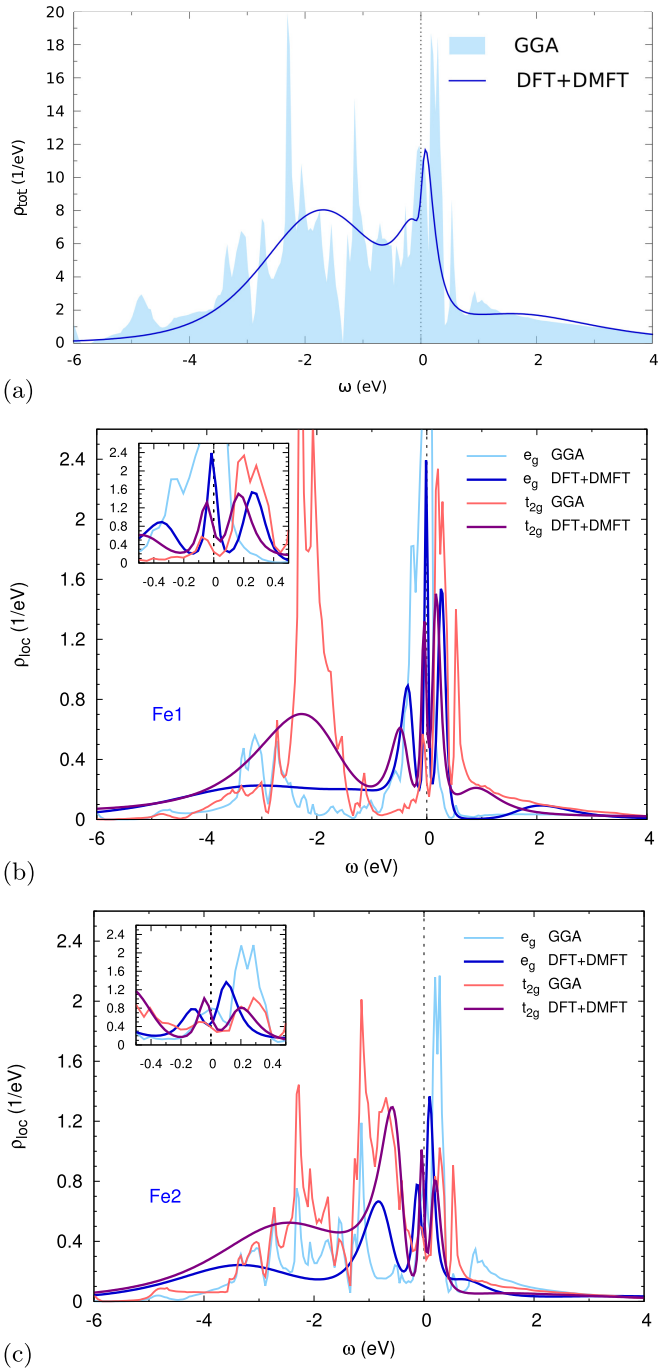

FIG. 4. Spectral functions of $D0_3$-Fe_3Al. (a) Total, (b) local Fe1, and (c) local Fe2. Insets in (b) and (c) are low-energy blowups.

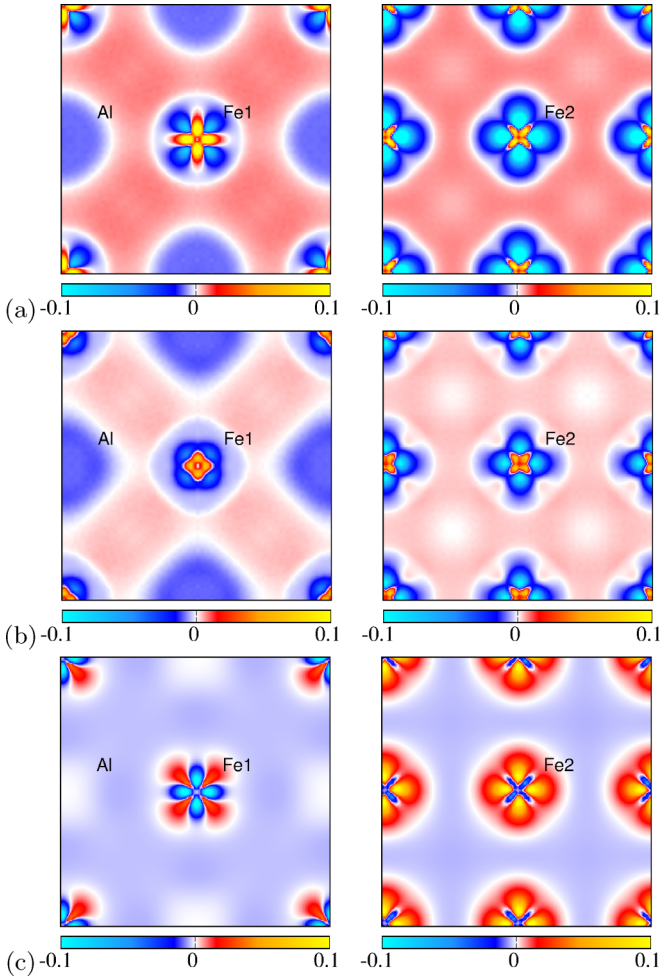

FIG. 5. Relevant charge-density plots in $D0_3$-Fe_3Al around Fe1 (left) and Fe2 (right) with the c axis perpendicular to the plotting plane. (a) GGA bonding charge density (see text). (b) DFT+DMFT bonding charge density. (c) Charge difference $n_{\mathrm{DFT+DMFT}} - n_{\mathrm{GGA}}$.

a more subtle orbital/directional electronic structure around Fe1, whereas Fe2 with its "washed-out" orbital signature looks similar to Fe in the $L1_2$ structure. A strong GGA favoring of e_g character at low energy in the case of Fe1 is weakened in DFT+DMFT, i.e., with correlations there are orbital-balancing tendencies at the Fermi level.

From the electron count, the Fe1(t_{2g}) states become strongly correlation enhanced, while on the other hand, the Fe2(e_g) electrons benefit from a local Coulomb interaction (cf. Table I). In principle, localizing $D0_3$ electrons in effective t_{2g} orbitals is understandable from a charge-repulsion argument due to the orbital direction. Because of the stronger hybridized environment on Fe2 imposed by the nearby Al, the single-site argument is not easily applicable there. Note that the effective e_g filling is leveled out in DFT+DMFT between Fe1 and Fe2. Figure 5 underlines the present findings by inspecting the intra- and intersite charge transfers. The bonding charge density $n^{\mathrm{bond}} \equiv n^{\mathrm{crystal}} - n^{\mathrm{atom}}$ with many-body effects shows, furthermore, a charge depletion in the interstitial bonding region compared to the GGA result. In total, also the Fe sites in the $D0_3$ structure gain $3d$ electrons upon the impact of local Coulomb interactions. While as expected the Fe2 site has a similar filling as the Fe site in $L1_2$, the Fe1 site has a lower electron count by roughly half an electron. Note that the absence of significant Fe filling differences with correlations in the recent work by Galler *et al.* [5] for $B2$-FeAl might be explained by the fact that no charge self-consistent framework was utilized in that study.

Concerning the correlation strength, though the Fe1 site and in general the e_g orbital character has a somewhat lower QP weight, there is neither a striking difference between the two Fe sublattices, nor between the e_g/t_{2g} character. In numbers, an average value of $Z \sim 0.8$ is slightly higher than

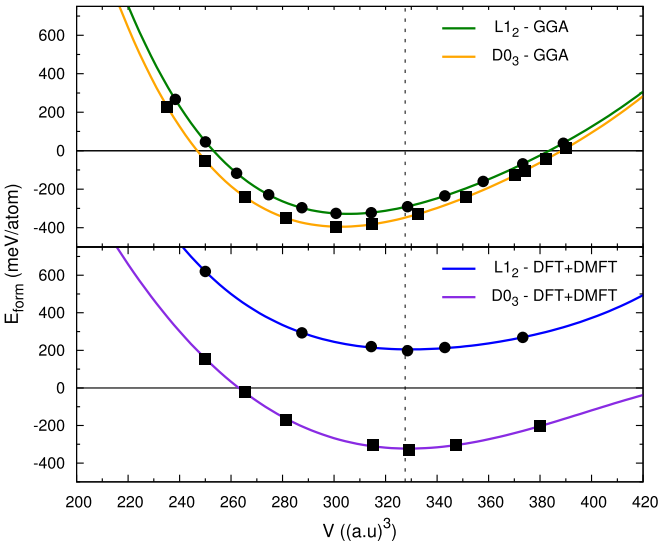

FIG. 6. Comparison of Fe_3Al formation-energy curves for the $D0_3$ and the $L1_2$ structure within NM-GGA and PM-DFT+DMFT. The dashed line marks the experimental equilibrium volume.

for the $L1_2$ structure, marking somewhat weaker correlation effects.

The Fe_3Al compound is not a particularly strongly correlated material, since the ratio of the local Coulomb interaction and the bandwidth is well below unity. In addition, the local Fe occupation ranging between seven and eight electrons is already above the optimal Hund's physics scenario [41–43] of about 5 ± 1 electrons (where, e.g., iron pnictides reside). Still, correlation effects are effective in modifying the charge density and the low-energy character, impacting the bonding properties as well as the charge and spin responses.

2. Energetics

We turn now to the structural phase competition between $D0_3$ and $L1_2$, by comparing the formation energy $E_{\rm form}$ per atom with respect to the volume V, i.e.,

$$E^{\rm Fe_3Al}_{{\rm form},m}(V) = E^{\rm Fe_3Al}_{{\rm tot},m}(V) - \tfrac{3}{4}E^{\rm bcc\text{-}Fe}_{{\rm tot},m}(V_{\rm eq}) - \tfrac{1}{4}E^{\rm fcc\text{-}Al}_{{\rm tot},m}(V_{\rm eq}), \quad (2)$$

where $V_{\rm eq}$ marks the respective equilibrium volume of the elemental phase. The additional common index m refers to the fact that each energy is given for the same magnetic state, e.g., NM, PM, or FM. Thus *explicit* magnetic formation/ordering terms do not enter our definition of $E_{\rm form}$. In that respect, the data shown in Fig. 6 are based on NM-GGA and PM-DFT+DMFT calculations. Both numerical schemes designate the $D0_3$ structure correctly as the stable one, with, however, two obvious differences. First, while in the many-body scheme the equilibrium volume is well reproduced, GGA yields a value too small by about 10%. Second, the energy difference $\Delta E^{L1_2}_{D0_3}$ between both structural types is about eight times larger within DFT+DMFT. Furthermore, the bulk modulus B is smaller in the latter scheme.

It was indeed shown in Ref. [11] that the first-principles description of the electronic structure and the phase stability of Fe_3Al is delicate. Upon ferromagnetic order, the $L1_2$ phase is by mistake stabilized in GGA(PBE). In this regard, a detailed data comparison is provided in Table II. While NM-GGA yields the correct qualitative structural hierarchy, the detailed structural data are off the experimental values. On the good side, introducing ferromagnetism on the GGA level brings the lattice constant and bulk modulus close to experiment. However, it not only misleadingly stabilizes the $L1_2$ structure [11], but now strongly underestimates the formation energy. This major difference from the experimental $E^{\rm Fe_3Al}_{\rm form}$ does not appear to be linked solely to the GGA functional, but due to a generally insufficient Kohn-Sham description of the magnetic energy in Fe-Al. Magnetism has been shown to be important for the $D0_3$ alloy ordering in that system [49]. Also in the LDA-based work by Watson and Weinert [50], a value $E^{\rm Fe_3Al}_{\rm form,FM} = -230$ meV/atom was obtained for spin-polarized $D0_3$-Fe_3Al. From the computation of the formation energy of various Fe compounds, the authors there concluded that introducing spin polarization in the Kohn-Sham exchange-correlation functional underestimates the magnetic energy for such alloys.

For comparison, we computed also the formation energy of FM-$D0_3$ within DFT+DMFT. The corresponding value $E^{\rm Fe_3Al}_{\rm form,FM} = -315$ meV/atom differs only slightly from the PM value. Thus the magnetic-ordering energy does not strongly influence the $D0_3$ ordering, when assuming coherent magnetic states. Of course, the *explicit* magnetic-ordering energy $E^{\rm Fe_3Al}_{\rm form,FM} - E^{\rm Fe_3Al}_{\rm form,PM} = -170$ meV/atom is still sizable. Concerning the competition between chemical orderings with PM *or* FM order in the Fe-Al phase diagram, this latter energy is surely relevant. A detailed statistical-mechanics study of this problem is, however, beyond the scope of the present work. For completeness, we provide in Table III the magnetic

TABLE II. Comparison of structural data for $D0_3$-Fe_3Al. Formation energy $E_{\rm form}$ (in meV/atom), bulk modulus B (in GPa), lattice constant (in a.u.), and stability against the $L1_2$ structure. The (NM,FM,PM) formation energies are computed using the corresponding (NM,FM,PM) total energy of bcc Fe [cf. Eq. (2)].

	$E_{\rm form}$	B	a	Stable
NM-GGA	-394	218	5.331	✓
FM-GGA	-202	151	5.465	↯
PM-DFT+DMFT	-325	143	5.480	✓
Experiment	-320 ± 20[a]	144[b]	5.473[c]	✓

[a]Reference [44].
[b]Reference [45].
[c]Reference [46].

TABLE III. Comparison of the Fe magnetic moments in ferromagnetic $D0_3$-Fe_3Al (in μ_B).

	$m_{\rm Fe1}$	$m_{\rm Fe2}$
FM-GGA	2.45	2.12
FM-DFT+DMFT	2.17	1.48
Experiment	2.18,[a] 2.12[b]	1.50,[a] 1.46[b]

[a]Reference [47].
[b]Reference [48].

moments in FM-$D0_3$. While GGA overestimates the local Fe moments, DFT+DMFT once more brings the data in line with experimental findings.

The results of the DFT+DMFT scheme are overall in very good agreement with the available experimental data. Note again that in order to evaluate the formation energy, the bcc Fe problem was of course also treated in DFT+DMFT, respectively, with the same magnetic state m and with identical local Coulomb interactions. Compared to NM-GGA, the less negative E_{form} of the $D0_3$ structure, in better agreement with experiment, matches the reduced bonding strength revealed from the correlated charge densities (cf. Fig. 5). For the case of $L1_2$-Fe_3Al, correlations not only render it much more energetically unfavorable compared to $D0_3$, but its formation energy becomes even positive, marking the compound unstable. This may be explained by the discussed correlation-induced weakening of the xz/yz states with a significant bonding-antibonding nature, compared to the strengthening of the xy and z^2 states. Thus many-body effects beyond conventional DFT do not merely lead to some quantitative changes, but display a *qualitative* effect on the energetics in the Fe-Al system.

The general improvement in the theoretical description of $D0_3$-Fe_3Al underlines not only the importance of electronic correlations, but renders it clear that a faithful description of the paramagnetic state is sufficient to account for the phase-relevant characterization.

B. Fe_2VAl

In the final section, we discuss the electronic structure of the Heusler $L2_1$-Fe_2VAl compound that emerges from $D0_3$-Fe_3Al by replacing the Fe1 sublattice with V atoms.

Figure 7 shows the total and local spectral properties, again by comparing GGA and DFT+DMFT. As in the earlier DFT-based studies [22,23], we find a semimetallic solution in the former Kohn-Sham calculation. A dichotomy is seen by inspecting the transition-metal electron-state characters on the local level. Below the Fermi level the low-energy region is dominated by Fe(t_{2g}) states, while above ε_F there are dominantly V(e_g) states. As expected because of replacing the Fe1 ions, the V site has a more pronounced orbital differentiation. Yet due to the different vanadium valence, the GGA filling is of course only a bit more than half the size of the Fe site.

Note that within DFT+DMFT we utilize the same U and J_H on the Fe and V sites. This choice can be motivated based on the strong intersite hybridizations in the given intermetallic system, leading to a coherent screening that minimizes substantial site differences in the local Coulomb interactions. With correlations, a clear gap structure emerges in the low-energy region, which is only fully realized at lower temperature. A pseudogap signature is obtained at a higher $T = 387$ K. It is notable that the spectral weight is shifted towards the low-energy region to form sharp gap edges. Thus the gap formation is not of obvious single-particle character and has similarities with, e.g., the (pseudo)gap structure in cuprates. Therefore, the insulating state is not of a conventional band-insulating semiconductor type. Measuring the charge gap from the middle of the gap-edge structure, a size $\Delta_g \sim 0.15$ eV is read off at $T = 193$ K. This is in excellent agreement with experimental values for a charge gap in Fe_2VAl [16].

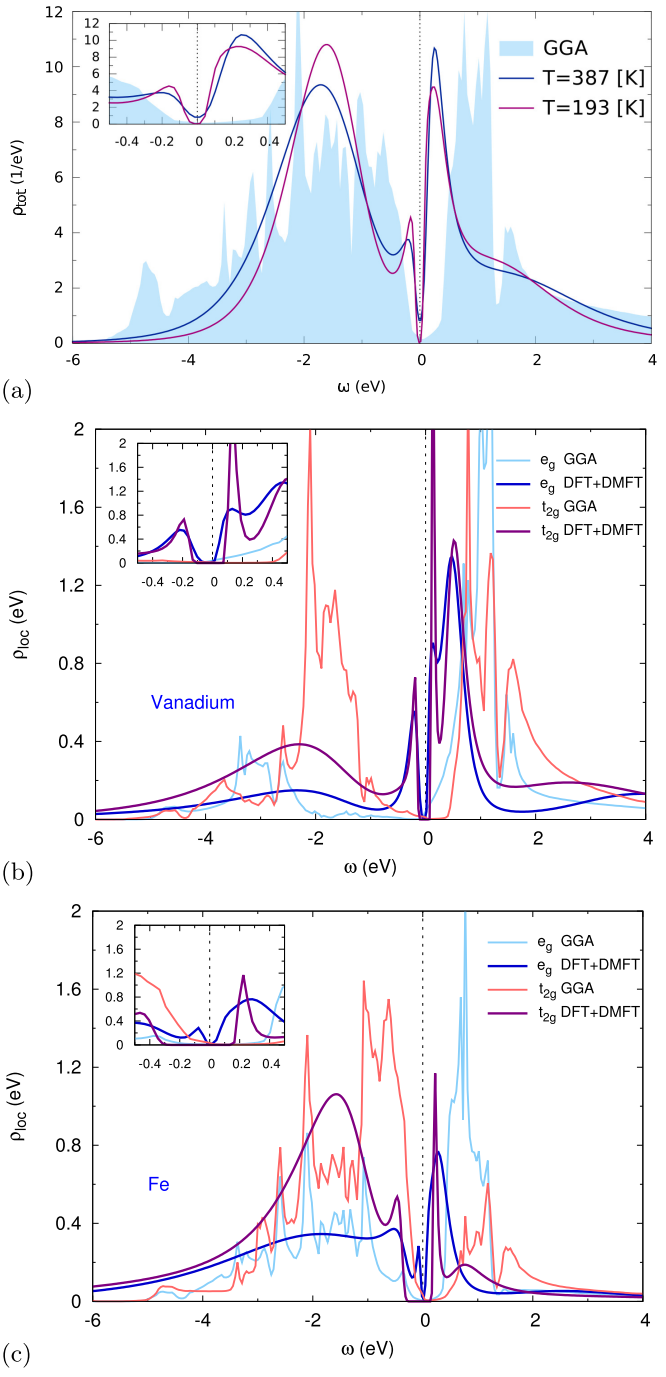

FIG. 7. Spectral function of $L2_1$-Fe_2VAl. Top: Total with DFT+DMFT for two different temperatures. Middle: V local. Bottom: Fe local.

Both transition-metal elements contribute to the intricate gap formation, but the V ion seems to play a more dominant role due to the larger spectral-function enhancement at the gap edges. Moreover, the low-energy spectra with correlations display a more balanced e_g,t_{2g} contribution compared to GGA. This is in line with a nearly orbital-independent local self-energy on the V sites. Therefrom, the correlation strength is enhanced on the latter sites in comparison to the Fe sites,

TABLE IV. Projected local-orbital occupations in Fe_2VAl for $T = 387$ K. The first rows are GGA, and the second rows are DFT+DMFT results, respectively.

		e_g		t_{2g}			
		x^2-y^2	z^2	xz	yz	xy	Total
$L2_1$	V	0.45	0.45	0.97	0.97	0.97	3.81
		0.70	0.70	0.90	0.90	0.90	4.10
	Fe	1.09	1.09	1.65	1.65	1.65	7.13
		1.45	1.45	1.72	1.72	1.72	8.06

yet the vanadium-based QP weight $Z \sim 0.7$ is again moderate. Needless to say, Fe_2VAl is of course no Mott insulator. Still, electronic correlations beyond conventional DFT are at the origin of the gap formation and gap opening. In this context, the different electron fillings of V and Fe are interesting (see Table IV). While the Fe ion unsurprisingly shows a very similar filling characteristic as the Fe2 ion in $D0_3$-Fe_3Al, the V ion already surely differs in the number of valence electrons. With an effective filling close to four electrons, the V site lies one hole below half filling, i.e., in a designated Hund's metal regime [41–43]. The orbital-resolved V occupations align somewhat in DFT+DMFT, however, it seems that the overall correlation strength due to the given sizes of the bandwidth and local Coulomb interactions is still too weak to drive very strong Hund's physics. But unconventional spin fluctuations could nonetheless play a relevant role in the enhanced experimental specific heat [19].

V. CONCLUSIONS

Recently, there have been various investigations that employ realistic DMFT approaches beyond Kohn-Sham DFT($+U$) to elemental iron and its alloy with aluminum. Studies on phase stabilities in the Fe phase diagram [51,52], on the α-Fe phonon spectrum [53], on vacancy formation in α-Fe [54], and on the magnetism in $B2$-FeAl [4,5] were performed. The present work adds a DFT+DMFT examination of the Fe_3Al and Fe_2VAl correlated electronic structure.

We show that although both compounds do not fall in the standard category of strongly correlated systems, more subtle many-body effects are still relevant for a correct description. The energetics and phase stability of Fe_3Al build upon such effects, by providing an improved value for the formation energy with a clear energy separation to the $L1_2$ structure. Note that the charge self-consistent version of the DFT+DMFT framework is important to elucidate such physics. Thereby, not only do local changes on the explicitly correlated lattice sites matter, but the overall charge redistributions including also the interstitial and ligand regions are crucial. On general grounds for cubic intermetallics, the open bcc lattice seems more adequate for correlated (Fe-based) compounds. For systems on a close-packed fcc lattice with sizable local Coulomb interactions, the local correlations become comparatively too strong, weakening important bonding properties. So, fcc-based compounds such as, e.g., Ni_3Al and Cu_3Au either do not display substantial *local* correlation physics or are well described in standard DFT. We want to note that the issue of chemical disorder is surely relevant concerning the phase stabilities close to the Fe_3Al composition of the Fe-Al phase diagram [55]. Treating such additional degrees of freedom together with the correlations encountered here beyond DFT is a formidable task which has to be faced in the future for a detailed thermodynamic understanding of Fe-Al.

The Fe_2VAl compound manifests an intriguing twist to traditional intermetallics, in the sense that the material is derived from the well-known Fe_3Al metal but displays an intricate gap opening reminiscent of (pseudo)gap physics observed in correlated oxides. The DFT+DMFT gap size and its sensitivity to temperature are in excellent agreement with experimental results for this compound. Since also Hund's physics may play a role on the vanadium site, this example shows how easily traditional material physics may be confronted with challenging mechanisms from strongly correlated matter. In a future work, addressing the thermoelectric properties of Fe_2VAl on the basis of the results established here would be highly interesting.

ACKNOWLEDGMENTS

We thank D. Grieger and M. Obermeyer for helpful discussions. This research was supported by DFG-FOR1346. Computations were performed at the University of Hamburg and at the North-German Supercomputing Alliance (HLRN) under Grant No. hhp00026.

[1] K. Miyatani and S. Iida, J. Phys. Soc. Jpn. **25**, 1008 (1968).
[2] B. I. Min, T. Oguchi, H. J. F. Jansen, and A. J. Freeman, J. Magn. Magn. Mater. **54–57**, 1091 (1986).
[3] P. Mohn, C. Persson, P. Blaha, K. Schwarz, P. Novák, and H. Eschrig, Phys. Rev. Lett. **87**, 196401 (2001).
[4] A. G. Petukhov, I. I. Mazin, L. Chioncel, and A. I. Lichtenstein, Phys. Rev. B **67**, 153106 (2003).
[5] A. Galler, C. Taranto, M. Wallerberger, M. Kaltak, G. Kresse, G. Sangiovanni, A. Toschi, and K. Held, Phys. Rev. B **92**, 205132 (2015).
[6] C. S. Lue, Y. Öner, D. G. Naugle, and J. H. Ross, Jr., Phys. Rev. B **63**, 184405 (2001).
[7] Z. Jagličić, S. Vrtnik, M. Feuerbacher, and J. Dolinšek, Phys. Rev. B **83**, 224427 (2011).
[8] M. Fallot, Ann. Phys. (Paris) **6**, 305 (1936).
[9] C. S. Wang, B. M. Klein, and H. Krakauer, Phys. Rev. Lett. **54**, 1852 (1985).
[10] P. Bagno, O. Jepsen, and O. Gunnarsson, Phys. Rev. B **40**, 1997(R) (1989).
[11] F. Lechermann, F. Welsch, C. Elsässer, C. Ederer, M. Fähnle, J. M. Sanchez, and B. Meyer, Phys. Rev. B **65**, 132104 (2002).
[12] F. Lechermann, M. Fähnle, B. Meyer, and C. Elsässer, Phys. Rev. B **69**, 165116 (2004).

[13] B. L. Gyorffy, A. J. Pindor, J. Staunton, G. M. Stocks, and H. Winter, J. Phys. F: Met. Phys. **15**, 1337 (1985).
[14] I. A. Abrikosov, A. V. Ponomareva, P. Steneteg, S. A. Barannikova, and B. Alling, Curr. Opin. Solid State Mater. Sci. **20**, 85 (2015).
[15] Y. Nishino, M. Kato, S. Asano, K. Soda, M. Hayasaki, and U. Mizutani, Phys. Rev. Lett. **79**, 1909 (1997).
[16] C. S. Lue and J. H. Ross, Jr., Phys. Rev. B **58**, 9763 (1998).
[17] H. Okamura, J. Kawahara, T. Nanba, S. Kimura, K. Soda, U. Mizutani, Y. Nishino, M. Kato, I. Shimoyama, H. Miura *et al.*, Phys. Rev. Lett. **84**, 3674 (2000).
[18] J. W. Allen, B. Batlogg, and P. Wachter, Phys. Rev. B **20**, 4807 (1979).
[19] C. S. Lue, J. H. Ross, Jr., C. F. Chang, and H. D. Yang, Phys. Rev. B **60**, R13941(R) (1999).
[20] Y. Nishino, S. Deguchi, and U. Mizutani, Phys. Rev. B **74**, 115115 (2006).
[21] M. Mikami, S. Tanaka, and K. Kobayashi, J. Alloys Compd. **484**, 444 (2009).
[22] D. J. Singh and I. I. Mazin, Phys. Rev. B **57**, 14352 (1998).
[23] R. Weht and W. E. Pickett, Phys. Rev. B **58**, 6855 (1998).
[24] D. I. Bilc and P. Ghosez, Phys. Rev. B **83**, 205204 (2011).
[25] D. Do, M.-S. Lee, and S. D. Mahanti, Phys. Rev. B **84**, 125104 (2011).
[26] S. Y. Savrasov, G. Kotliar, and E. Abrahams, Nature (London) **410**, 793 (2001).
[27] L. V. Pourovskii, B. Amadon, S. Biermann, and A. Georges, Phys. Rev. B **76**, 235101 (2007).
[28] D. Grieger, C. Piefke, O. E. Peil, and F. Lechermann, Phys. Rev. B **86**, 155121 (2012).
[29] S. G. Louie, K. M. Ho, and M. L. Cohen, Phys. Rev. B **19**, 1774 (1979).
[30] B. Meyer, C. Elsässer, F. Lechermann, and M. Fähnle, FORTRAN 90 Program for Mixed-Basis-Pseudopotential Calculations for Crystals (unpublished).
[31] A. N. Rubtsov, V. V. Savkin, and A. I. Lichtenstein, Phys. Rev. B **72**, 035122 (2005).
[32] P. Werner, A. Comanac, L. de' Medici, M. Troyer, and A. J. Millis, Phys. Rev. Lett. **97**, 076405 (2006).
[33] O. Parcollet, M. Ferrero, T. Ayral, H. Hafermann, I. Krivenko, L. Messio, and P. Seth, Comput. Phys. Commun. **196**, 398 (2015).
[34] P. Seth, I. Krivenko, M. Ferrero, and O. Parcollet, Comput. Phys. Commun. **200**, 274 (2016).
[35] J. P. Perdew, K. Burke, and M. Ernzerhof, Phys. Rev. Lett. **77**, 3865 (1996).
[36] B. Amadon, F. Lechermann, A. Georges, F. Jollet, T. O. Wehling, and A. I. Lichtenstein, Phys. Rev. B **77**, 205112 (2008).
[37] V. I. Anisimov, D. E. Kondakov, A. V. Kozhevnikov, I. A. Nekrasov, Z. V. Pchelkina, J. W. Allen, S.-K. Mo, H.-D. Kim, P. Metcalf, S. Suga *et al.*, Phys. Rev. B **71**, 125119 (2005).
[38] M. Aichhorn, L. Pourovskii, V. Vildosola, M. Ferrero, O. Parcollet, T. Miyake, A. Georges, and S. Biermann, Phys. Rev. B **80**, 085101 (2009).
[39] K. Haule, C.-H. Yee, and K. Kim, Phys. Rev. B **81**, 195107 (2010).
[40] M. Karolak, T. O. Wehling, F. Lechermann, and A. I. Lichtenstein, J. Phys.: Condens. Matter **23**, 085601 (2011).
[41] P. Werner, E. Gull, M. Troyer, and A. J. Millis, Phys. Rev. Lett. **101**, 166405 (2008).
[42] K. Haule and G. Kotliar, New J. Phys. **11**, 025021 (2009).
[43] L. de' Medici, J. Mravlje, and A. Georges, Phys. Rev. Lett. **107**, 256401 (2011).
[44] P. D. Desai, J. Phys. Chem. Ref. Data **16**, 109 (1987).
[45] G. Simmons and H. Wang, *Single Crystal Elastic Constants and Calculated Aggregated Properties* (MIT Press, Cambridge, MA, 1971).
[46] W. B. Pearson and G. H. Vineyard, *A Handbook of Lattice Spacings and Structures of Metals and Alloys* (Pergamon, Oxford, UK, 1958).
[47] S. J. Pickart and R. Nathans, Phys. Rev. **123**, 1163 (1961).
[48] D. Satula, L. Dobrzyński, A. Malinowski, K. Szymański, and J. Waliszweski, J. Magn. Magn. Mater. **151**, 211 (1995).
[49] J. Kudrnovský, V. Drchal, L. Bergqvist, J. Rusz, I. Turek, B. Újfalussy, and I. Vincze, Phys. Rev. B **90**, 134408 (2014).
[50] R. E. Watson and M. Weinert, Phys. Rev. B **58**, 5981 (1998).
[51] I. Leonov, A. I. Poteryaev, V. I. Anisimov, and D. Vollhardt, Phys. Rev. Lett. **106**, 106405 (2011).
[52] L. V. Pourovskii, T. Miyake, S. I. Simak, A. V. Ruban, L. Dubrovinsky, and I. A. Abrikosov, Phys. Rev. B **87**, 115130 (2013).
[53] I. Leonov, A. I. Poteryaev, V. I. Anisimov, and D. Vollhardt, Phys. Rev. B **85**, 020401(R) (2012).
[54] P. Delange, T. Ayral, S. I. Simak, M. Ferrero, O. Parcollet, S. Biermann, and L. Pourovskii, Phys. Rev. B **94**, 100102(R) (2016).
[55] B. Sundman, I. Ohnuma, N. Dupin, U. R. Kattner, and S. G. Fries, Acta Mater. **57**, 2896 (2009).